

# Stimuli-Responsive Nanostructured Viologen-Siloxane Materials for Controllable Conductivity

**Citation for published version (APA):**

van den Bersselaar, B. W. L., van de Ven, A. P. A., de Waal, B. F. M., Meskers, S. C. J., Eisenreich, F., & Vantomme, G. (2024). Stimuli-Responsive Nanostructured Viologen-Siloxane Materials for Controllable Conductivity. *Advanced Materials*, 36(23), Article 2312791. <https://doi.org/10.1002/adma.202312791>

**Document license:**  
CC BY

**DOI:**  
[10.1002/adma.202312791](https://doi.org/10.1002/adma.202312791)

**Document status and date:**  
Published: 06/06/2024

**Document Version:**  
Publisher's PDF, also known as Version of Record (includes final page, issue and volume numbers)

**Please check the document version of this publication:**

- A submitted manuscript is the version of the article upon submission and before peer-review. There can be important differences between the submitted version and the official published version of record. People interested in the research are advised to contact the author for the final version of the publication, or visit the DOI to the publisher's website.
- The final author version and the galley proof are versions of the publication after peer review.
- The final published version features the final layout of the paper including the volume, issue and page numbers.

[Link to publication](#)

**General rights**

Copyright and moral rights for the publications made accessible in the public portal are retained by the authors and/or other copyright owners and it is a condition of accessing publications that users recognise and abide by the legal requirements associated with these rights.

- Users may download and print one copy of any publication from the public portal for the purpose of private study or research.
- You may not further distribute the material or use it for any profit-making activity or commercial gain
- You may freely distribute the URL identifying the publication in the public portal.

If the publication is distributed under the terms of Article 25fa of the Dutch Copyright Act, indicated by the "Taverne" license above, please follow below link for the End User Agreement:

[www.tue.nl/taverne](http://www.tue.nl/taverne)

**Take down policy**

If you believe that this document breaches copyright please contact us at:

[openaccess@tue.nl](mailto:openaccess@tue.nl)

providing details and we will investigate your claim.

# Stimuli-Responsive Nanostructured Viologen-Siloxane Materials for Controllable Conductivity

Bart W. L. van den Bersselaar, Alex P. A. van de Ven, Bas F. M. de Waal, Stefan C. J. Meskers, F. Eisenreich,\* and G. Vantomme\*

Spontaneous phase separation is a promising strategy for the development of novel electronic materials, as the resulting well-defined morphologies generally exhibit enhanced conductivity. Making these structures adaptive to external stimuli is challenging, yet crucial as multistate reconfigurable switching is essential for neuromorphic materials. Here, a modular and scalable approach is presented to obtain switchable phase-separated viologen-siloxane nanostructures with sub-5 nm features. The domain spacing, morphology, and conductivity of these materials can be tuned by ion exchange, repeated pulsed photoirradiation and electric stimulation. Counterion exchange triggers a postsynthetic modification in domain spacing of up to 10%. Additionally, in some cases, 2D to 1D order–order transitions are observed with the latter exhibiting a sevenfold decrease in conductivity with respect to their 2D lamellar counterparts. Moreover, the combination of the viologen core with tetraphenylborate counterions enables reversible and in situ reduction upon light irradiation. This light-driven reduction provides access to a continuum of conducting states, reminiscent of long-term potentiation. The repeated voltage sweeps improve the nanostructures alignment, leading to increased conductivity in a learning effect. Overall, these results highlight the adaptivity of phase-separated nanostructures for the next generation of organic electronics, with exciting applications in smart sensors and neuromorphic devices.

## 1. Introduction

Stimuli-responsive materials capable of transitioning between a broad range of tunable states constitute a promising class of materials for smart sensors and information storage.<sup>[1–3]</sup> Many examples of materials comprising bistable states that act as binary “on”- and “off”-states have been reported, however their design does not cover multi-level switching tuned by stimulus dosage.<sup>[4]</sup> Yet, multistate switching is ubiquitous in nature, exemplified by ionic channels in neurons that exhibit different levels of conductance, enabling the fine-tuning of synaptic transmission and modulation of neuronal communication.<sup>[5,6]</sup> Inspired by such systems, multistate memory devices have been developed, the switching mechanisms of which rely on redox reaction, slow kinetics and charge trapping.<sup>[7]</sup> However, variation of the conductivity in such systems is often disconnected from their morphologies due to the lack of adaptivity in covalent polymers, which limits the achievable complexity therein.

Therefore, organic oligomeric materials that are perfectly defined at the molecular level are a recent target in next-generation

nanotechnology as molecular structures can be directly linked to macromolecular properties.<sup>[8]</sup> Typically, these ordered materials show enhanced electronic properties compared to their disordered counterparts as a result of the decreased number of grain boundaries.<sup>[9,10]</sup> Specifically, organic materials comprising well-defined 1D and 2D morphologies are of great interest for energy transfer and optoelectronics.<sup>[11–14]</sup> An effective strategy to create versatile nanostructured organic materials is based on sidechain engineering.<sup>[15–17]</sup> In the past, discrete oligodimethylsiloxane (oDMS,  $\bar{D} < 1.00001$ ) have been introduced in end-functionalized molecules, which self-assemble into 2D materials.<sup>[18,19]</sup> These phase-separated structures are exploited to translate molecular events to a macromolecular level, exemplified by diphenylanthracene-based molecules that exhibit a hundredfold increase in photon-upconversion in an ordered material compared to its disordered counterpart.<sup>[20]</sup> However, such phase-separated block molecules typically exhibit transitions from 1D to 2D morphologies as a function of

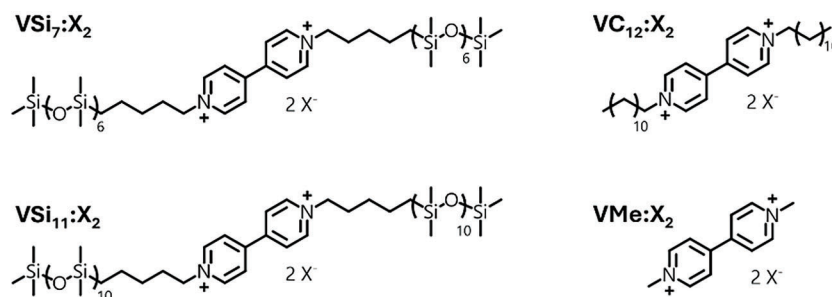
B. W. L. van den Bersselaar, A. P. A. van de Ven, B. F. M. de Waal, S. C. J. Meskers, F. Eisenreich, G. Vantomme  
 Institute for Complex Molecular Systems and Laboratory of Macromolecular and Organic Chemistry  
 Eindhoven University of Technology  
 P.O. Box 513, Eindhoven 5600 MB, The Netherlands  
 E-mail: [f.eisenreich@tue.nl](mailto:f.eisenreich@tue.nl); [g.vantomme@tue.nl](mailto:g.vantomme@tue.nl)

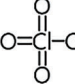

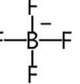
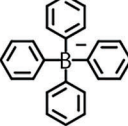
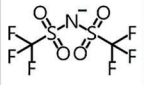





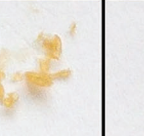


F. Eisenreich  
 Polymer Performance Materials Group  
 Department of Chemical Engineering and Chemistry  
 Eindhoven University of Technology  
 P.O. Box 513, Eindhoven 5600 MB, The Netherlands

 The ORCID identification number(s) for the author(s) of this article can be found under <https://doi.org/10.1002/adma.202312791>

© 2024 The Authors. Advanced Materials published by Wiley-VCH GmbH. This is an open access article under the terms of the [Creative Commons Attribution](https://creativecommons.org/licenses/by/4.0/) License, which permits use, distribution and reproduction in any medium, provided the original work is properly cited.

DOI: 10.1002/adma.202312791



Name	VSi <sub>7</sub> :Cl <sub>2</sub>	VSi <sub>7</sub> :Br <sub>2</sub>	VSi <sub>7</sub> :I <sub>2</sub>	VSi <sub>7</sub> :(ClO <sub>4</sub> ) <sub>2</sub>	VSi <sub>7</sub> :(PF <sub>6</sub> ) <sub>2</sub>	VSi <sub>7</sub> :(BF <sub>4</sub> ) <sub>2</sub>	VSi <sub>7</sub> :(Ph <sub>4</sub> B) <sub>2</sub>	VSi <sub>7</sub> :TFSI <sub>2</sub>
X <sup>-</sup>	Cl <sup>-</sup>	Br <sup>-</sup>	I <sup>-</sup>					
Image								

**Figure 1.** Chemical structures of block molecules included in this work and overview of VSi<sub>7</sub>:X<sub>2</sub> with counterion structures and physical appearance.

temperature.<sup>[21]</sup> Contrary, applications such as semiconductors, transistors, and memristors require tunable electronic properties at operating temperature, hence fueling the need for additional stimuli to modulate morphologies other than heat.<sup>[22–24]</sup> Preferably, multistimuli responsive materials are developed, due to their increased complexity.<sup>[25]</sup>

In this light, an intriguing class of organic molecules are viologens.<sup>[26]</sup> Due to their three distinct and (meta)stable redox states with low reduction potentials, viologens are ideal electron-acceptors for electronic applications.<sup>[27,28]</sup> Subsequent one- or twofold reduction of the viologens increases the electron density on the bipyridium center, and consequently the conductivity is enhanced in a step-wise fashion.<sup>[29,30]</sup> Recently, reduction of a viologen displayed formation of a stable dimer due to electrostatic interactions yielding large resistive on/off ratios.<sup>[31]</sup> Furthermore, Forbes et al. showed that the coordination of a tetraphenylborate counterion (Ph<sub>4</sub>B<sup>-</sup>) to the viologen allows for photon induced electron transfer.<sup>[32,33]</sup> Since excitation of the Ph<sub>4</sub>B<sup>-</sup> ion into its singlet excited state leads to electron transfer from the phenyl ring to the viologen, light can be used as an external stimulus to in situ reduce the viologen core whilst oxidizing the tetraphenylborate. The spatiotemporal control granted by the use of light makes the coordination pair of a viologen with Ph<sub>4</sub>B<sup>-</sup> counterions a promising class of materials for targeted multistate switching.

Although well-defined phase separation, stimuli-responsiveness, and tunable conductivity individually are of great interest for the development of new functional materials, the synergistic use of all three components in a single system is rare. Here, we present a novel set of functional materials that combines all these factors in a singular system. We report

a modular approach to prepare a library of viologen-based materials (**Figure 1**) that spontaneously phase separate into well-defined structures and their emerging electronic properties were investigated. We display how facile counterion exchange enables postsynthetic modification of both the nanostructures as well as the electronic properties. Moreover, the conductivity of the material was reversibly switched between “off”- and a continuum of “on”-states using photoinduced reduction of the viologen. Temporal control over both the reduction and the back electron transfer was obtained by modulating the light intensity and presence of oxygen. Finally, we show that alignment of the 2D nanostructures enhances the conductivity of VSi<sub>7</sub>:(Ph<sub>4</sub>B)<sub>2</sub>, stressing the importance of well-defined structures for cognitive materials.

## 2. Results and Discussion

The chemical structures of the synthesized viologen-derivatives and their counterions are displayed in **Figure 1**. We prepared viologen-centered block molecules with two different lengths of oligodimethylsiloxane (VSi<sub>7</sub>:X<sub>2</sub> and VSi<sub>11</sub>:X<sub>2</sub>), respectively, and alkyl-substituted reference compounds VC<sub>12</sub>:X<sub>2</sub> and VMe:X<sub>2</sub>, where X is the counterion. Thereby, both the phase-separated structures as well as the degree to which the sidechains interdigitate can be investigated. The most common counterions for viologens with (opto-)electronic applications were used to explore their effect on the phase-separated structures and the emerging properties.<sup>[26]</sup>

To obtain the library of viologen-centered block molecules, firstly Si<sub>7</sub>H and Si<sub>11</sub>H were reacted with 5-bromo-1-pentene via a palladium catalyzed hydrosilylation in high yields (85–95%).

**Table 1.** Properties of  $\text{VSi}_7\text{:X}_2$  block molecules.

Entry	Counterion	Physical appearance	$\varphi_{\text{non-oDMS}}^{\text{a}}$ (-)	Morph. <sup>b)</sup>	$d^{\text{c}}$ (nm)
$\text{VSi}_7\text{:TFSI}_2$	TFSI <sup>-</sup>	Brown wax	0.34	Lam	3.8
$\text{VSi}_7\text{:}(\text{Ph}_4\text{B})_2$	$\text{Ph}_4\text{B}^-$	Orange sticky solid	0.46	Lam	3.8
$\text{VSi}_7\text{:Br}_2$	Br <sup>-</sup>	Yellow brittle solid	0.24	Lam	4.0
$\text{VSi}_7\text{:I}_2$	I <sup>-</sup>	Red brittle solid	0.35	Lam	4.0
$\text{VSi}_7\text{:}(\text{PF}_6)_2$	$\text{PF}_6^-$	White sticky solid	0.25	Lam	4.2
$\text{VSi}_7\text{:}(\text{BF}_4)_2$	$\text{BF}_4^-$	White brittle solid	0.22	Col <sub>h</sub>	3.7
$\text{VSi}_7\text{:Cl}_2$	Cl <sup>-</sup>	Brown sticky wax	0.26	Col <sub>h</sub>	3.9
$\text{VSi}_7\text{:}(\text{ClO}_4)_2$	$\text{ClO}_4^-$	Ochre wax	0.22	Col <sub>h</sub>	4.0

<sup>a)</sup>  $\varphi_{\text{non-oDMS}}$  defined as the volume fraction of the non-oDMS part of the material and determined using the volume of the unit cell of the respective crystal structure of  $\text{VMe:X}_2$  as reported in the CCDC, a volume of  $80 \text{ mL mol}^{-1}$  for each  $\text{C}_5\text{H}_{10}$  linker and a volume of  $552 \text{ mL mol}^{-1}$  for each  $\text{Si}_7$  chain; <sup>b)</sup> Morphology of the nanostructure was determined from the relative positions of the Bragg reflection peaks with respect to the primary reflection ( $q^*$ ). Lamellar morphologies show reflections spaced integers apart ( $q^*$ ,  $2q^*$ ,  $3q^*$ , ...) whereas columnar phases show reflections at  $q^*$ ,  $\sqrt{3}q^*$ ,  $2q^*$ ,  $\sqrt{7}q^*$ ,  $3q^*$ , ...; <sup>c)</sup> Domain spacing of the morphology determined using  $d = 2\pi/q^*$ .

Subsequently, these products were subjected to a Menshutkin reaction with 4,4'-bipyridine in acetonitrile. Consecutive extraction and recrystallization yielded  $\text{VSi}_7\text{:Br}_2$  and  $\text{VSi}_{11}\text{:Br}_2$  on a multi-gram scale in 53–70% yield. The purity was confirmed using  $^1\text{H}$  and  $^{13}\text{C}$  NMR spectroscopy as well as MALDI-TOF-mass spectrometry (Figures S1–S6, Supporting Information).  $\text{VC}_{12}\text{:Br}_2$  was synthesized as reported in literature.<sup>[34]</sup>

The counterion exchange was performed by stirring a concentrated solution of  $\text{VSi}_7\text{:Br}_2$  in acetone with an excess of the respective sodium salt upon which a clear color change was visible, indicative of the formation of a different charge-transfer (CT) pair.<sup>[35]</sup> Extraction of the block molecule from the aqueous phase yielded  $\text{VSi}_7\text{:X}_2$  comprising eight different counterions (Table 1, see details in the Supporting Information). The complete counterion exchange was confirmed using X-ray photoelectron spectroscopy (XPS), indicated by the disappearance of the characteristic  $\text{Br}_{3p}$  peaks after a reaction time of 1–18 h (Figure 2A). Detailed analysis of the full spectra confirmed the high purity of  $\text{VSi}_7\text{:X}_2$  (Figure S7, Supporting Information).

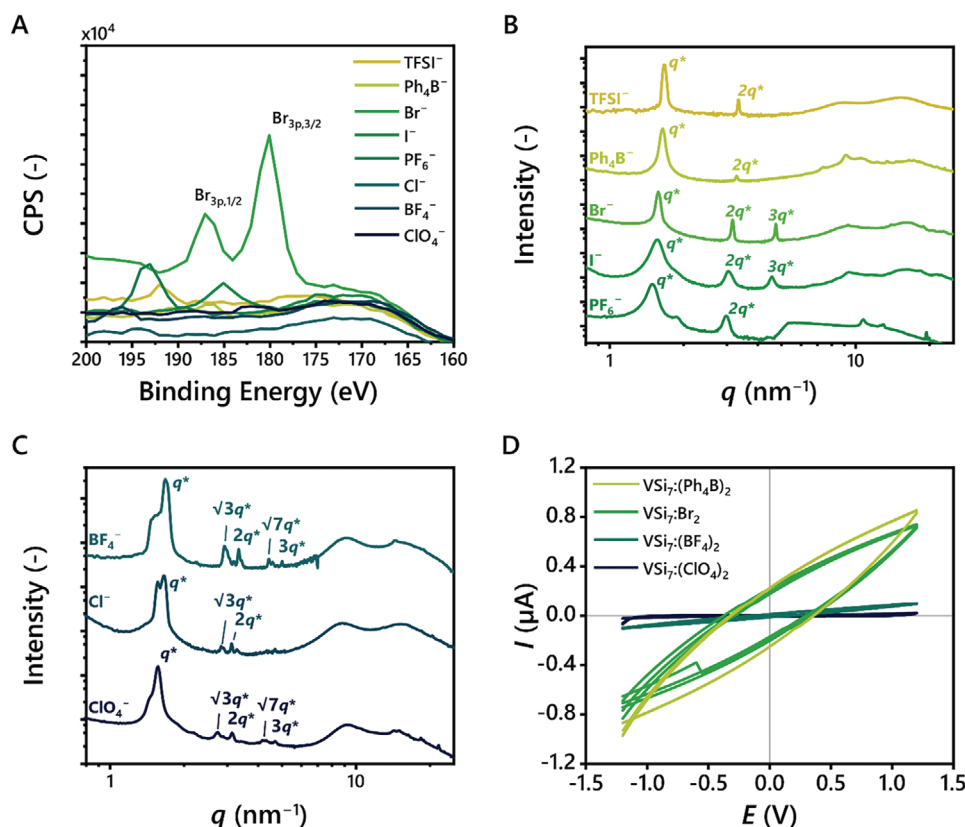
Since viologens are known to exhibit a different packing in their crystalline unit cell based on the associated counterion, it was expected that the morphology of the block molecules also varies with the counterion.<sup>[36–40]</sup> Thereto, the phase separation of  $\text{VSi}_7\text{:X}_2$  was investigated using medium- and wide angle X-ray spectroscopy (MAXS/WAXS, Figure 2B,C). These spectra were recorded on unannealed samples, as no melting and crystallization events were observed using differential scanning calorimetry (DSC, Figures S8 and S9, Supporting Information). Only  $\text{VSi}_7\text{:}(\text{ClO}_4)_2$  and  $\text{VSi}_7\text{:Cl}_2$  showed the presence of weak glass transition temperatures of around  $95^\circ\text{C}$ .  $\text{VSi}_7\text{:Br}_2$  was shown to phase separate into a lamellar morphology with a domain spacing ( $d_{\text{lam}}$ ) of 4.0 nm, which is slightly shorter than the calculated stretched length of the block molecule of 4.2 nm. This discrepancy indicated that the sidechains were partially interdigitated, which was corroborated by the fact that both  $\text{VSi}_{11}\text{:Br}_2$  and  $\text{VSi}_{11}\text{:}(\text{Ph}_4\text{B})_2$  show an increase in  $d_{\text{lam}}$  with respect to  $\text{VSi}_7\text{:Br}_2$  and  $\text{VSi}_7\text{:}(\text{Ph}_4\text{B})_2$  smaller than the calculated length of eight additional oDMS units (Figure S10A, Supporting Information). Inspection of the scattering pattern of  $\text{VC}_{12}\text{:Br}_2$  showed that the material was highly crystalline without long-range ordering, under-

lining the importance of oDMS to obtain phase-separated structures (Figure S11, Supporting Information). Similar to  $\text{VSi}_7\text{:Br}_2$ , lamellar morphologies were found for  $\text{VSi}_7\text{:TFSI}_2$ ,  $\text{VSi}_7\text{:}(\text{Ph}_4\text{B})_2$ ,  $\text{VSi}_7\text{:I}_2$ , and  $\text{VSi}_7\text{:}(\text{PF}_6)_2$ . Surprisingly, a change in domain spacing was observed upon counterion exchange. The maximum  $d_{\text{lam}}$  was found for  $\text{VSi}_7\text{:}(\text{PF}_6)_2$  ( $d_{\text{lam}} = 4.2 \text{ nm}$ ), which matched the calculated stretched length of the block molecule. Counterion exchange from  $\text{PF}_6^-$  to  $\text{TFSI}^-$  allows for postsynthetic modification of the domain spacing of 10% (from 4.2 to 3.8 nm). To achieve such an alteration via covalent chemistry the siloxane content would require a 15% change. We rationalize that the change in  $d_{\text{lam}}$  originates from different crystalline packing of the viologen. Due to the amorphous character of the oDMS pendants, single crystals of  $\text{VSi}_7\text{:X}_2$  cannot be obtained. Hence, we analyzed previously reported crystal structures of  $\text{VMe:X}_2$ , which revealed different free volume for the sidechains, whilst retaining the 2D intramolecular stacking required for lamellar morphology (Figures S12 and S13, Supporting Information).<sup>[36–40]</sup> Next to a change in  $d_{\text{lam}}$ , it was also found that three block molecules with chloride, perchlorate and tetrafluoroborate counterions spontaneously phase separated into a columnar hexagonal packing (Figure 2D). We hypothesize that this change from 2D to 1D morphologies also originates from the crystalline packing of the viologen. Close inspection of the crystal structures revealed that viologen-counterion combinations that result in lamellar ordering exhibit intramolecular stacking in two dimensions (Figures S12 and S13, Supporting Information).<sup>[40–42]</sup> Contrarily, the crystal structures of viologens with  $\text{Cl}^-$ ,  $\text{ClO}_4^-$ , and  $\text{Ph}_4\text{B}^-$  counterions contained such interactions only in one direction, explaining their phase separation into columnar morphologies.

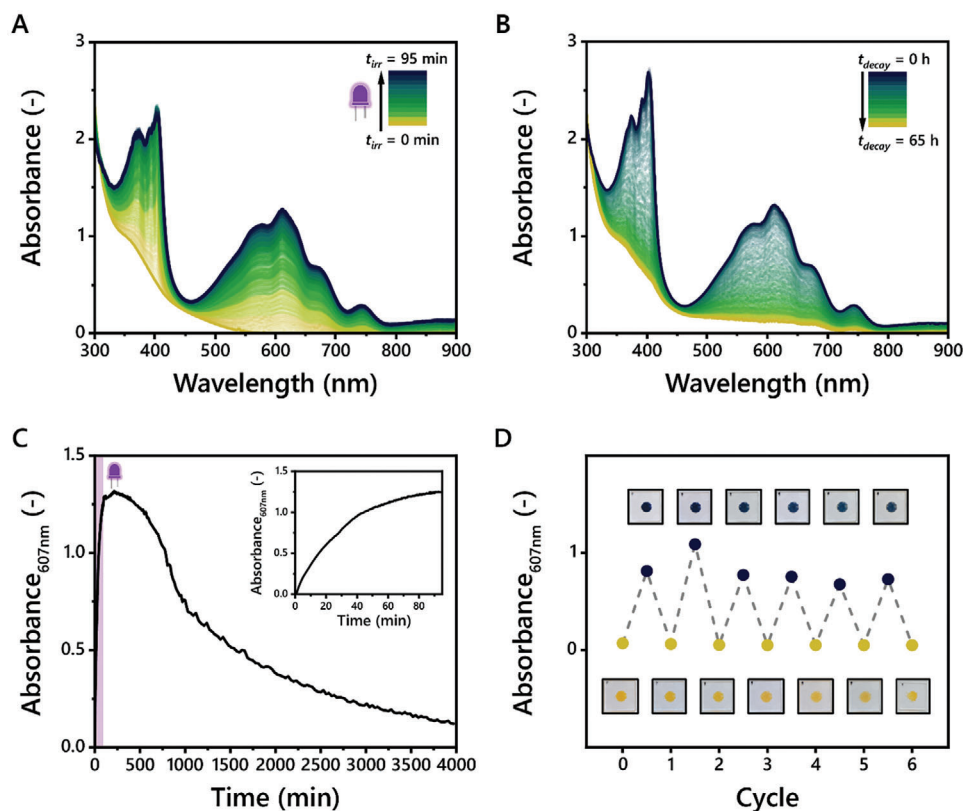
The redox potentials of the viologens were determined using cyclic voltammetry in solution, showing that the oDMS sidechain had no influence on the redox potential of the bipyridinium (Figure S14A–F, Supporting Information). Moreover, multi-cycle voltammetry experiments using  $\text{VSi}_7\text{:}(\text{Ph}_4\text{B})_2$  revealed excellent stability of the redox switching up to 100 cycles (Figure S14G, Supporting Information). To further explore the structure–function relationship of these block molecules, the current–voltage characteristics of several  $\text{VSi}_7\text{:X}_2$  were studied in bulk to determine their conductivity (Figure 2D). Hereto, the block molecules were pressed between two ITO covered quartz slides

equipped with UV-light curable glue containing 20  $\mu\text{m}$  spacers to obtain an active area of 0.3–1.3  $\text{cm}^2$  (Figure S15, Supporting Information). A voltage sweep was performed from  $-1.2$  to  $1.2$  V in steps of 0.05 V with a scanning speed of 0.6  $\text{V s}^{-1}$  and the color of the viologen was monitored during this process. As the different redox states of viologens have distinct colors, the absence of color change was a good indication that these voltage sweeps did not electrochemically reduce the bulk of the viologen. Secondly, we observed that the  $I/V$ -curves of  $\text{VSi}_7\text{:Br}_2$  and  $\text{VSi}_7\text{:}(\text{Ph}_4\text{B})_2$  did not pass through the origin. This effect is most likely due to the displacement of counterions related to the capacitance of the cell involving electrolytic and electrochemical contributions. The  $I/V$ -curves of the columnar ordered  $\text{VSi}_7\text{:}(\text{BF}_4)_2$  and  $\text{VSi}_7\text{:}(\text{ClO}_4)_2$  passed closer through the origin, indicating lower capacitance characteristics in these materials. Conductivity was deduced from the slope of the  $I/V$ -curves and we found that the 2D-nanostructured  $\text{VSi}_7\text{:Br}_2$  and  $\text{VSi}_7\text{:}(\text{Ph}_4\text{B})_2$  exhibit an increase in conductivity (0.24–0.09  $\mu\text{S m}^{-1}$ ) with respect to the columnar  $\text{VSi}_7\text{:}(\text{BF}_4)_2$  and  $\text{VSi}_7\text{:}(\text{ClO}_4)_2$  (0.04–0.01  $\mu\text{S m}^{-1}$ ). Since the domain spacings as determined using MAXS/WAXS are smaller than the thickness of the layer (20  $\mu\text{m}$ ), we argue that the charge transport is percolative in nature. We rationalize that the 2D morphologies exhibit higher conductivity than their 1D-counterparts due to the charge trapping and coulomb blockade effects that are known to severely limit charge transport in quasi 1D conductors.

The reported photoinduced reduction of a viologen in  $\text{VMe}:(\text{Ph}_4\text{B})_2$  prompted us to investigate the influence of illumination on the conductivity in  $\text{VSi}_7\text{:}(\text{Ph}_4\text{B})_2$ .<sup>[33]</sup> The formation of a metastable reduced viologen can take place via photoinduced electron transfer between the bipyridium center and the  $\text{Ph}_4\text{B}^-$  counterion, provided that the reaction partners are in close proximity ( $<3$  Å).<sup>[32]</sup> Inspection of the WAXS spectra of  $\text{VSi}_7\text{:}(\text{Ph}_4\text{B})_2$  revealed a peak at  $q = 20$   $\text{nm}^{-1}$ , which corresponds to roughly 3 Å, which is absent in  $\text{VSi}_7\text{:Br}_2$  (Figure S10B, Supporting Information). Hence, the reaction partners are in close enough proximity for photoinduced electron transfer to occur. Hereafter,  $\text{VSi}_7\text{:}(\text{Ph}_4\text{B})_2$  was sandwiched between two quartz slides to form a uniform layer with a thickness of 10  $\mu\text{m}$ . The UV-vis spectrum was recorded at intervals of 15 s, whilst constantly irradiating ( $\lambda_{\text{irr}} = 405$  nm) the sample for 95 min (Figure 3A). A clear change in the UV-vis spectrum was observed with the appearance of two bands centered at 402 and 607 nm. Visually, a color change of the sample from yellow to deep blue occurred, indicative of the formation of the radical cation.<sup>[32]</sup> When the increase in intensity around 607 nm levelled off after 95 min of irradiation, the light source was turned off and the decay of the radical cation was monitored in the dark (Figure 3B). The disappearance of the aforementioned characteristic peaks at 402 and 607 nm was evident. Close observation of the intensity at 607 nm revealed that the radical cation had a lifetime of several days in ambient atmosphere (Figure 3C). The decay is mediated



**Figure 2.** A) XPS graphs of  $\text{VSi}_7\text{:X}_2$  showing the disappearance of  $\text{Br}_{3p}$  peaks upon counterion exchange. B,C) MAXS/WAXS scattering profiles of  $\text{VSi}_7\text{:X}_2$  block molecules with lamellar morphology (B) and columnar morphology (C). D)  $I/V$ -curves of  $\text{VSi}_7\text{:X}_2$  with various counterions. Conductivity was derived from the slope of the curve and the active area of the cell. In the legends of all figures, the counterions  $\text{X}^-$  of the block molecules  $\text{VSi}_7\text{:X}_2$  are indicated.

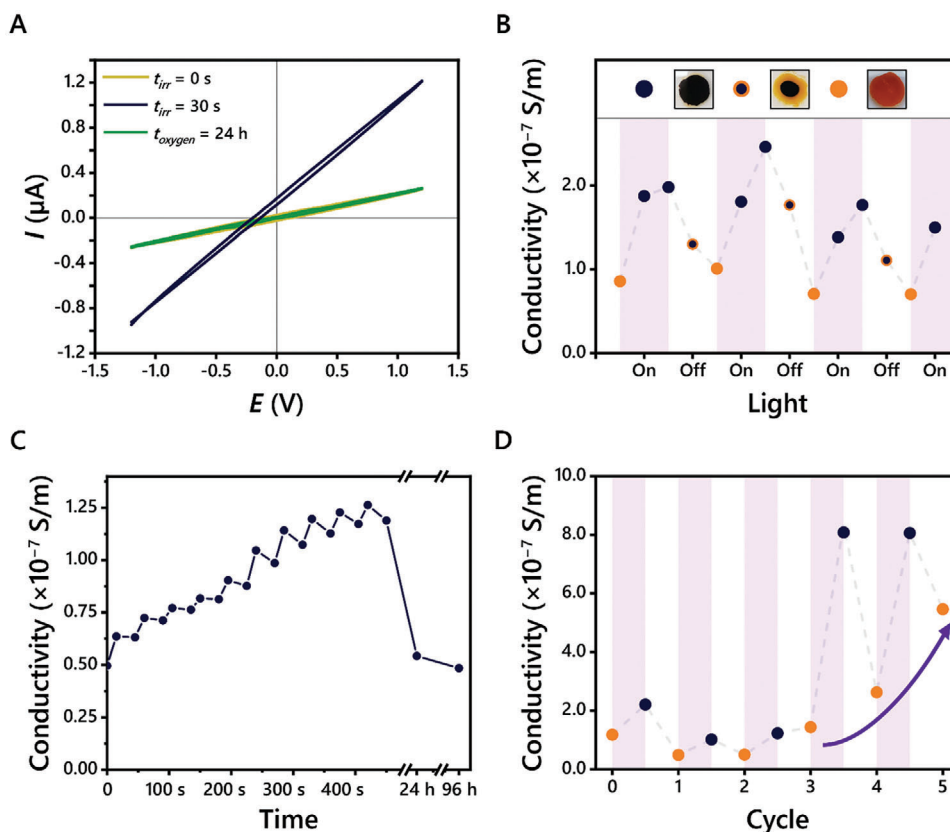


**Figure 3.** Solid-state UV-vis measurement of  $\text{VSi}_7:(\text{Ph}_4\text{B})_2$  between quartz slides (thickness = 10  $\mu\text{m}$ ). A) UV-vis spectra measured every 15 s under constant irradiation ( $\lambda_{\text{irr}} = 405 \text{ nm}$ ,  $E = 12 \text{ mW cm}^{-2}$ ). B) UV-vis spectra of the thermal decay of  $\text{VSi}_7:(\text{Ph}_4\text{B})_2$ . C) Absorbance at the absorption maximum of the radical cation (607 nm) monitored over time. The purple segment represents the irradiation period of 90 min. The inset shows a zoom-in of the increase in absorbance during irradiation. D) Multiple cycles of irradiation/decay of  $\text{VSi}_7:(\text{Ph}_4\text{B})_2$  between quartz slides. Insets show color change upon reduction/oxidation of  $\text{VSi}_7:(\text{Ph}_4\text{B})_2$ . The sample was irradiated for 15 s ( $\lambda_{\text{irr}} = 405 \text{ nm}$ ,  $E = 230 \text{ mW cm}^{-2}$ ) and the back electron transfer was accelerated by placing the cell in an oxygen-rich atmosphere.

by diffusion of oxygen into the cell, as apparent from the radial pattern of the color loss. Moreover, samples prepared under inert atmosphere in a glovebox retained their blue color for at least several weeks, stressing the importance of oxygen in the decay process of the radical cation. UV-vis studies of  $\text{VSi}_7:(\text{Ph}_4\text{B})_2$  in dilute solutions showed spectral changes similar to those of reference compound  $\text{VMe}:(\text{Ph}_4\text{B})_2$  upon irradiation, indicating that the radical formation herein is consistent with literature (Figure S16, Supporting Information).<sup>[32]</sup> Importantly, the characteristic absorption bands of the radical appeared only upon irradiation of  $\text{VSi}_7:(\text{Ph}_4\text{B})_2$  and were not visible in control experiments with  $\text{VSi}_7:(\text{BF}_4)_2$  (Figure S16F, Supporting Information). During the decay, a new absorption maximum around 450 nm appears, which we hypothesize to originate from liberation of the tetraphenylborate radical in dilute solution, as proposed in the mechanism by Forbes et al.<sup>[33]</sup> Comparing the decay of the radical cation of  $\text{VSi}_7:(\text{Ph}_4\text{B})_2$  with the decay of the radical cation  $\text{VMe}:(\text{Ph}_4\text{B})_2$  in solution, we find that the half-life time of the radical cation of the siloxane derivative is roughly 50% longer. The increased radical stability in the block molecule is expected to result from steric hindrance due to the additional  $\sigma\text{DMS}$  chain.

Since reduction of viologens is known to enhance their conductivity, we envisioned that step-wise irradiation of  $\text{VSi}_7:(\text{Ph}_4\text{B})_2$

leads to switchable conductivity states. This hypothesis was strengthened by the solid-state UV-vis measurements, since each data point in Figure 3C depicts a different amount of radical cation formed and thus a different conductivity. To evaluate this possibility, the ITO-cells were irradiated during 30 s and their  $I/V$ -curves recorded (Figure 4A; Figure S17A, Supporting Information). An increase in conductivity showed that the radical cation of  $\text{VSi}_7:(\text{Ph}_4\text{B})_2$  is already formed after 30 s of irradiation. When the cell was stored in an oxygen-rich atmosphere, the radical cation was oxidized and returned to the dication state within 24 h. However, when the device was left in ambient air, the back electron transfer process took up to one week (Figure S17A, Supporting Information). Moreover, control experiments using  $\text{VSi}_7:(\text{BF}_4)_2$  did not display this change in conductivity (Figure S17B, Supporting Information), hence underlining the importance of the  $\text{Ph}_4\text{B}^-$  counterion in the reduction process. Thermal effects during the reduction of  $\text{VSi}_7:(\text{Ph}_4\text{B})_2$  were excluded by monitoring the temperature increase upon irradiation, which was found to be minimal (increase of 5  $^\circ\text{C}$  after 40 s of irradiation, Figure S18, Supporting Information). MAXS/WAXS spectra confirmed that irradiation had not disrupted the lamellar packing of the material, and that the CT-distance between viologen and counterion remained unchanged (Figure S19, Supporting Information).



**Figure 4.** A)  $I/V$ -curves of  $\text{VSi}_7:(\text{Ph}_4\text{B})_2$  before irradiation (yellow), after irradiation of 30 s (blue) and after 24 h in an oxygen-rich atmosphere (green) ( $\lambda_{\text{irr}} = 405 \text{ nm}$ ,  $E = 230 \text{ mW cm}^{-2}$ , thickness =  $20 \mu\text{m}$ ,  $A = 0.8 \text{ cm}^2$ ). B) Conductivity upon irradiation of  $\text{VSi}_7:(\text{Ph}_4\text{B})_2$  for 15 s (twice) and subsequent decay of the radical for one week. Inset figures show the color change at different times during the experiment. C) Long-term potentiation of  $\text{VSi}_7:(\text{Ph}_4\text{B})_2$  by 15 s pulsed irradiation, followed by 30 s lag time before the next pulse. D) Conductivity of  $\text{VSi}_7:(\text{Ph}_4\text{B})_2$  during multiple cycles of irradiation (irradiation for 15 s (twice) and subsequent decay of the radical for one week). After numerous voltage sweeps, the conductivity of the dication state increased.

To test the stability of the switching process, the ITO cell was subsequently subjected to several irradiation cycles (Figure 4B; Figure S20A, Supporting Information). For each cycle,  $\text{VSi}_7:(\text{Ph}_4\text{B})_2$  was irradiated twice with a 15 s pulse of 405 nm light and the conductivity was determined after each pulse. The sample was then left to undergo back electron transfer and its conductivity was recorded after one day and after one week. Here, the vital role of oxygen diffusion was again apparent, as visible from the radial color pattern in the inset of Figure 4B. The results of these experiments show that the aforementioned reversibility in the switching of  $\text{VSi}_7:(\text{Ph}_4\text{B})_2$  also results in reversible states with varying conductivity.

To push the limits of this system in the generation of multiple conducting states, we tested pulsed light irradiation with short increments of consecutive 15 s light pulses, followed by 30 s lag time (Figure 4C; Figure S20B, Supporting Information). From these experiments we find that pulsed light irradiation results in a continuum of conductive states, indicated by the small changes ( $<0.1 \times 10^{-7} \text{ S m}^{-1}$ ) between the states. Nevertheless, we show that different levels of conductivity can be targeted by matching the irradiation time to the desired outcome. Thereafter, conductivity decreases after each pulse, due to the back electron transfer process mentioned above. Moreover, Figures 3A and 4C show that the timescale of the in-situ reduction is controlled by

the intensity of the light ( $E = 12$  vs  $230 \text{ mW cm}^{-2}$ , respectively). Next, the back electron transfer is controlled by the presence of oxygen. These two parameters allow us to control the “on”- and “off”-switching of the system by exposure to light and oxygen.

Surprisingly, upon repetition of multiple cycles (irradiation for  $2 \times 15 \text{ s}$ , followed by radical decay of one week) we found that the conductivity of the dicationic species increased from cycle 2 to cycle 5 by 360% (Figure 4D, also visible after 200 s in Figure 4C). In stark contrast, a negligible increase of 1.5% in conductivity was observed after performing multiple cycles on a fresh device without light irradiation (Figure S21, Supporting Information). To understand the nature of this “learning” effect, we studied changes in the nanomorphology of  $\text{VSi}_7:(\text{Ph}_4\text{B})_2$  before and after pulsed light irradiation in the device. Hereto, grazing incidence medium/wide angle X-Ray spectroscopy (GiMAXS/WAXS) was performed on a fresh sample of  $\text{VSi}_7:(\text{Ph}_4\text{B})_2$  as well as on a sample that underwent pulsed light irradiation and voltage sweeps. We prepared the fresh sample by pressing the material between two ITO-covered quartz slides and subsequent removal of the top slide. Similarly, for the material that was exposed to light and voltage sweeps we removed the top ITO-electrode and measured GiMAXS/WAXS on the material that remained on the bottom slide. We found that both samples were phase-separated into a lamellar morphology, proving that neither the irradiation nor

applied potential disrupted the 2D morphology (Figure S22, Supporting Information). Next, we probed the relative orientation of the block molecule to the ITO substrate. Here, close inspection of the normalized intensity of the primary Bragg reflections as a function of azimuth angles showed that  $\text{VSi}_7:(\text{Ph}_4\text{B})_2$  from the device exhibited a more pronounced peak at  $180^\circ$  (Figure S22, Supporting Information). This position of the peak intensity indicates that the lamellar domains were oriented preferentially parallel to the substrate. In contrast, fresh  $\text{VSi}_7:(\text{Ph}_4\text{B})_2$  showed a more randomly oriented lamellar morphology on the substrate, with a full width half maximum (FWHM) value of  $22^\circ$  versus  $4^\circ$  in the aligned sample. This fivefold decrease in FWHM shows that the enhanced conductivity of  $\text{VSi}_7:(\text{Ph}_4\text{B})_2$  over cycles of pulsed irradiation goes in concert with an improved orientation of the lamellae parallel to the substrate. We rationalize that this effect originates from a progressive alignment of the dipole moment of  $\text{VSi}_7:(\text{Ph}_4\text{B})_2$  with the electric field. These results bring insights into the intriguing prospect of mechanisms of learning into materials, where repeated input leads to structural modification and improved function.<sup>[43]</sup>

### 3. Conclusion

We have demonstrated a scalable approach to synthesize a library of viologen-based block molecules that phase separate into well-ordered morphologies. Easy exchange of counterions enables postsynthetic simultaneous modification of the morphology and conductivity of the viologen. Moreover,  $\text{VSi}_7:(\text{Ph}_4\text{B})_2$  was in situ reduced upon irradiation, revealing its tunable electronic properties, where the reduction is regulated by light exposure and the state retention by storage of the device under inert atmosphere. Finally, the conductivity of the “off”-state increased after several voltage sweeps, which was explained by the analysis of the material orientation. This research adds a new strategy to the toolbox for tuning the electronic properties in organic nanomaterials as it allows for control over an extremely long-lived radical cation with enhanced conductivity compared to its dicationic state. By exploiting the phase separation into sub-5 nm domains, the molecular changes in conductivity of the viologen is translated to a macroscopic device. Besides, the conductivity of these materials was altered using counterion exchange, light, and alignment of the 2D morphologies using an electric field. Therefore, such systems allow the use of orthogonal stimuli to control the morphology and emerging function, whereas conventional organic devices typically rely on one process.<sup>[7]</sup> These findings underline the potential of these systems in advanced (opto-)electronic materials.

### Supporting Information

Supporting Information is available from the Wiley Online Library or from the author.

### Acknowledgements

The authors gratefully acknowledge Prof. E. W. Meijer for fruitful discussion regarding the experiments and the manuscript. P. A. A. Bartels is acknowledged for his help with the XPS experiments. This work was financially supported by the Dutch Research Council (OCENW.M20.256),

the Dutch Ministry of Education, Culture and Science (Gravity program 024.005.020) as well as the Alexander von Humboldt foundation for providing a Feodor Lynen research fellowship.

### Conflict of Interest

The authors declare no conflict of interest.

### Data Availability Statement

The data that support the findings of this study are available in the supplementary material of this article.

### Keywords

counterion exchange, molecular self-assembly, multistate switching, photoinduced electron transfer, stimuli-responsive

Received: November 27, 2023

Revised: February 1, 2024

Published online: March 7, 2024

- [1] B. L. Feringa, W. F. Jager, B. de Lange, *Tetrahedron* **1993**, 49, 8267.
- [2] L. Hu, Q. Zhang, X. Li, M. J. Serpe, *Mater. Horiz.* **2019**, 6, 1774.
- [3] K. Lou, Z. Hu, H. Zhang, Q. Li, X. Ji, K. Lou, Z. Hu, H. Zhang, Q. Li, X. Ji, *Adv. Funct. Mater.* **2022**, 32, 2113274.
- [4] Y. Cao, M. Derakhshani, Y. Fang, G. Huang, C. Cao, Y. Cao, M. Derakhshani, Y. Fang, C. Cao, G. Huang, *Adv. Funct. Mater.* **2021**, 31, 2106231.
- [5] S. G. Cull-Candy, M. M. Usowicz, *Nature* **1987**, 325, 525.
- [6] G. Voglis, N. Tavernarakis, *EMBO Rep.* **2006**, 7, 1104.
- [7] Y. Van De Burgt, A. Melianas, S. T. Keene, G. Malliaras, A. Salleo, *Nat. Electron.* **2018**, 1, 386.
- [8] G. M. Whitesides, B. Grzybowski, *Science* **2002**, 295, 2418.
- [9] G. De Luca, W. Pisula, D. Credgington, E. Treossi, O. Fenwick, G. M. Lazzerini, R. Dabirian, E. Orgiu, A. Liscio, V. Palermo, K. Müllen, F. Cacialli, P. Samori, *Adv. Funct. Mater.* **2011**, 21, 1279.
- [10] Y. F. Yao, P. Samori, L. Zhang, E. Orgiu, *Adv. Mater.* **2019**, 31, 1900599.
- [11] M. O’Neill, S. M. Kelly, *Adv. Mater.* **2011**, 23, 566.
- [12] F. Yang, S. Cheng, X. Zhang, X. Ren, R. Li, H. Dong, W. Hu, *Adv. Mater.* **2018**, 30, 1702415.
- [13] X. Zhan, A. Facchetti, S. Barlow, T. J. Marks, M. A. Ratner, M. R. Wasielewski, S. R. Marder, *Adv. Mater.* **2011**, 23, 268.
- [14] X. Zhuang, Y. Mai, D. Wu, F. Zhang, X. Feng, X. Zhuang, Y. Mai, D. Wu, F. Zhang, X. Feng, *Adv. Mater.* **2015**, 27, 403.
- [15] J. Mei, D. H. Kim, A. L. Ayzner, M. F. Toney, Z. Bao, *J. Am. Chem. Soc.* **2011**, 133, 20130.
- [16] J. Liu, L. Qiu, G. Portale, S. Torabi, M. C. A. Stuart, X. Qiu, M. Koopmans, R. C. Chiechi, J. C. Hummelen, L. J. Koster Anton, *Nano Energy* **2018**, 52, 183.
- [17] H. Sakaino, S. C. J. Meskers, E. W. Meijer, G. Vantomme, *Chem. Commun.* **2022**, 58, 12819.
- [18] W. Zhang, W. Yang, H. Pan, X. Lyu, A. Xiao, D. Liu, Y. Liu, Z. Shen, H. Yang, X. H. Fan, *Soft Matter* **2022**, 18, 3430.
- [19] B. Oschmann, J. Lawrence, M. W. Schulze, J. M. Ren, A. Anastasaki, Y. Luo, M. D. Nothling, C. W. Pester, K. T. Delaney, L. A. Connal, A. J. McGrath, P. G. Clark, C. M. Bates, C. J. Hawker, *ACS Macro Lett.* **2017**, 6, 668.
- [20] M. H. C. Son, A. M. Berghuis, F. Eisenreich, B. Waal, G. Vantomme, J. G. Rivas, E. W. Meijer, *Adv. Mater.* **2020**, 32, 2004775.



- [21] B. A. G. Lamers, R. Graf, B. F. M. De Waal, G. Vantomme, A. R. A. Palmans, E. W. Meijer, *J. Am. Chem. Soc.* **2019**, *141*, 15456.
- [22] T. Sarkar, K. Lieberth, A. Pavlou, T. Frank, V. Mailaender, I. McCulloch, P. W. M. Blom, F. Torricelli, P. Gkoupidenis, *Nat. Electron.* **2022**, *5*, 774.
- [23] Y. Van De Burgt, E. Lubberman, E. J. Fuller, S. T. Keene, G. C. Faria, S. Agarwal, M. J. Marinella, A. Alec Talin, A. Salleo, *Nat. Mater.* **2017**, *16*, 414.
- [24] G. A. Leith, C. R. Martin, A. Mathur, P. Kittikhunnatham, K. C. Park, N. B. Shustova, *Adv. Energy Mater.* **2022**, *12*, 2100441.
- [25] A. Goulet-Hanssens, F. Eisenreich, S. Hecht, *Adv. Mater.* **2020**, *32*, 1905966.
- [26] K. Madasamy, D. Velayutham, V. Suryanarayanan, M. Kathiresan, K. C. Ho, *J. Mater. Chem. C* **2019**, *7*, 4622.
- [27] L. Striepe, T. Baumgartner, *Chem. – Eur. J.* **2017**, *23*, 16924.
- [28] K. W. Shah, S. X. Wang, D. X. Y. Soo, J. Xu, *Polymers* **2019**, *11*, 1839.
- [29] J. Li, S. Pudar, H. Yu, S. Li, J. S. Moore, J. Rodríguez-López, N. E. Jackson, C. M. Schroeder, *J. Phys. Chem. C* **2021**, *125*, 21862.
- [30] W. W. Porter, T. P. Vaid, *J. Org. Chem.* **2005**, *70*, 5028.
- [31] Y. Han, C. Nickle, Z. Zhang, H. P. A. G. Astier, T. J. Duffin, D. Qi, Z. Wang, E. del Barco, D. Thompson, C. A. Nijhuis, *Nat. Mater.* **2020**, *19*, 843.
- [32] W. G. Santos, D. S. Budkina, V. M. Deflon, A. N. Tarnovsky, D. R. Cardoso, M. D. E. Forbes, *J. Am. Chem. Soc.* **2017**, *139*, 7681.
- [33] W. G. Santos, D. S. Budkina, P. F. G. M. da Costa, D. R. Cardoso, A. N. Tarnovsky, M. D. E. Forbes, *Mater. Adv.* **2022**, *3*, 3862.
- [34] B. Nieto-Ortega, J. Villalva, M. Vera-Hidalgo, L. Ruiz-González, E. Burzurí, E. M. Pérez, *Angew. Chem., Int. Ed.* **2017**, *56*, 12240.
- [35] P. M. S. Monk, N. M. Hodgkinson, R. D. Partridge, *Dyes Pigm.* **1999**, *43*, 241.
- [36] H. Tahara, Y. Furue, C. Suenaga, T. Sagara, *Cryst. Growth Des.* **2015**, *15*, 4735.
- [37] G. J. Moody, R. K. Owusu, A. M. Z. Slawin, N. Spencer, J. F. Stoddart, J. D. R. Thomas, D. J. Williams, *Angew. Chem., Int. Ed.* **1987**, *26*, 890.
- [38] I. Y. Polishchuk, L. G. Grineva, A. P. Polishchuk, A. N. Chernega, *Zh. Obshch. Khim.* **1966**, *66*, 1530.
- [39] F. Huang, K. A. Switek, L. N. Zakharov, F. R. Fronczek, C. Slebodnick, M. Lam, J. A. Golen, W. S. Bryant, P. E. Mason, A. L. Rheingold, M. Ashraf-Khorassani, H. W. Gibson, *J. Org. Chem.* **2005**, *70*, 3231.
- [40] J. H. Russell, S. C. Wallwork, *Acta Cryst. B* **1972**, *28*, 1527.
- [41] Y. L. Dou, Z. G. Li, J. W. Xu, W. X. Zhang, *Acta Cryst. E* **2007**, *63*, o1874.
- [42] F. Yang, J. C. Deng, Z. G. Li, J. W. Xu, *Acta Cryst. E* **2008**, *64*, o253.
- [43] J. S. Van Der Burgt, F. Scalerandi, J. J. De Boer, S. A. Rigter, E. C. Garnett, *Adv. Funct. Mater.* **2022**, *32*, 2203771.